Mikada, H., Moore, G.F., Taira, A., Becker, K., Moore, J.C., and Klaus, A. (Eds.)
Proceedings of the Ocean Drilling Program, Scientific Results Volume 190/196

18. Data Report: Permeabilities of Nankai Accretionary Prism Sediments[1]

Kusali Gamage[2] and Elizabeth Screaton[2]

ABSTRACT

Vertical permeability testing was conducted on 10 whole-round core samples collected from Sites 1173 and 1174 from Ocean Drilling Program Leg 190. Constant-flow permeability tests were conducted to estimate permeability values for selected core samples from the upper and lower Shikoku Basin facies. The highest permeability measured was 6.43×10^{-17} m^2 at a depth of 200 meters below seafloor (mbsf) at Site 1173 and the lowest permeability measured was 3.5×10^{-19} m^2 at a depth of 795 mbsf at Site 1174.

INTRODUCTION

Permeability is an important hydrologic component in quantitatively evaluating sediment consolidation and pore pressures. In clay-rich sediments, the intrinsic permeability generally decreases with decreasing porosity. In this study we used core samples from the Ocean Drilling Program (ODP) Leg 190, Sites 1173 and 1174 from the upper and lower Shikoku Basin facies of the Nankai accretionary prism (Fig. F1). Both sites were drilled along the Muroto Transect through the décollement zone or its equivalent (Moore, Taira, Klaus, et al., 2001). Site 1173 is located 11 km seaward of the deformation front and it represents the undeformed incoming sediments, whereas Site 1174 represents sediments within the proto-thrust zone (Moore et al., 2001). Although the Nankai accretionary complex is characterized by turbidite-rich sediments, the core samples from the Shikoku Basin facies are

F1. Location map, p. 7.

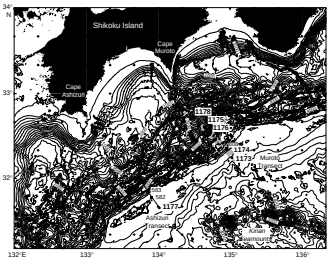

[1]Gamage, K., and Screaton, E., 2003. Data report: Permeabilities of Nankai accretionary prism sediments. *In* Mikada, H., Moore, G.F., Taira, A., Becker, K., Moore, J.C., and Klaus, A. (Eds.), *Proc. ODP, Sci. Results,* 190/196, 1–22 [Online]. Available from World Wide Web: <http://www-odp.tamu.edu/publications/190196SR/VOLUME/CHAPTERS/213.PDF>. [Cited YYYY-MM-DD]
[2]Department of Geological Sciences, University of Florida, 241 Williamson, Box 112120, Gainesville FL 32611, USA. Correspondence author: **kusali@ufl.edu**

Initial receipt: 20 November 2002
Acceptance: 22 April 2003
Web publication: 22 August 2003
Ms 190SR-213

composed of hemipelagic muds. To measure the vertical permeability of the sediments, constant-flow tests were conducted on core samples.

METHODS

Constant-flow permeability tests were used to estimate hydraulic conductivity values for selected core samples from ODP Sites 1173 and 1174 from the lower Shikoku Basin. The constant-flow approach pumps fluid into and out of the sample, and the resulting hydraulic gradient is measured. The constant-flow permeability tests were conducted using the Trautwein Soil Testing Equipment Company's DigiFlow K (Figs. F2, F3).

The equipment consists of the cell (to contain the sample and provide isostatic effective stress) and three pumps (sample top pump, sample bottom pump, and cell pump). Bladder accumulators were used to allow deionized water as the fluid in the pumps while using an idealized solution of seawater (25 g NaCl + 8 g $MgSO_4$ per liter of water) as the permeant throughout the sample. ASTM designation D 5084-90 (1990) was used as a guideline for general procedures.

The Leg 190 core samples were stored in plastic core liners and sealed with wax to prevent moisture loss. The samples were stored in water in the refrigerator at 4°C until immediately prior to sample preparation. Immediately before testing, cores were trimmed on both ends using a wire saw or a utility knife, depending on the lithology of the core, to fit within the flexible wall membrane. The samples had a minimum diameter of 2 in and sample heights varied from 2.5 to 3.8 in. The ends of every sample were trimmed to provide freshly exposed surfaces. After placing the sample within the flexible membrane, the samples were fitted with filter paper and saturated porous disks and the sample diameter and height were measured. The sample was placed in the cell, which was filled with deionized water so that the membrane-encased sample was completely surrounded by fluid. A small confining pressure of ~0.03 MPa (5 psi) was applied to fully saturate the sample. Flow lines were flushed with deionized water to remove trapped air bubbles. The sample was backpressured at ~0.28 MPa (40 psi) in order to fully saturate the sample. Backpressure was achieved by concurrently ramping the cell pressure and the sample pressure to maintain a steady effective stress. Saturation was verified by measuring the ratio of change in pore water pressure in the porous material to the change in the confining pressure (ASTM, 1990). Once the sample reached saturation, the cell fluid pressure was increased while the sample backpressure was maintained, thus increasing the effective stress on the sample. The maximum stress that the cell is able to sustain is ~1.03 MPa (150 psi), limiting the maximum effective stress to ~0.75 MPa (110 psi). Once the target effective stress was achieved, cell pressure and backpressure were maintained. The sample was allowed to equilibrate for at least 4 hr and generally overnight. Throughout the testing, vertical sample displacement and change in cell fluid volume were monitored.

Once the target effective stress level was achieved, a brief constant-pressure gradient test was conducted to select an appropriate flow rate for the subsequent constant-flow tests. During the constant-flow tests, flow rates were maintained by the top and bottom pumps, one on each end of the sample, ensuring that the volume of the sample is unchanged. During the permeation step, the head gradient was monitored to assure that gradients were not excessive (ASTM, 1990). Since fluid

F2. Laboratory setup, p. 8.

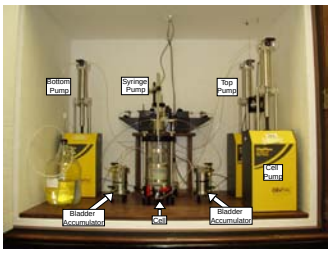

F3. Constant-flow closed system, p. 9.

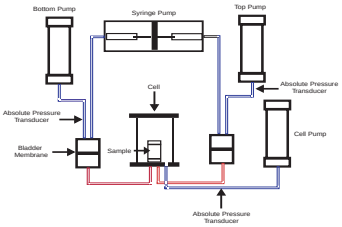

pressure in the closed hydraulic system is affected by temperature changes, testing was conducted within a closed cabinet with a fan to keep the internal temperature uniform. Temperature was monitored throughout the testing phase. For highly consolidated samples with low hydraulic conductivities, the Harvard apparatus PHD 2000 syringe pump was used to conduct very low flow rates, instead of the top and bottom pumps. The PHD 2000 consists of two syringes that can simultaneously pump fluid in and out of the sample at a specified flow rate.

Two to three constant-flow tests were performed at each effective stress level. Once permeability values were obtained, cell pressure was increased and the sample was allowed to equilibrate overnight at the new effective stress. At least two different effective stress steps were performed for each sample. If the permeability of the sample decreased significantly during permeation from the first effective stress step to the second effective stress step, then an extra effective stress step was performed.

Assuming hydrostatic pore fluid pressures, estimated depths at effective stress equal to 0.75 MPa at Sites 1173 and 1174 were 80 and 100 meters below seafloor (mbsf), respectively. Thus, applied effective stress levels used in the laboratory are likely to be well below in situ values. However, previous permeability studies (e.g., Bolton and Maltman, 1998; Bolton et al., 2000) have shown that the largest decrease in permeability occurred as effective stress were increased from 0 to 0.1 MPa; subsequently, permeabilities remained relatively constant. Therefore, we used the permeability results from the highest effective stress, and the values presented in this study represent the maximum in situ vertical permeabilities.

Using these measurements, the specified flow rate, Q (in cubic meters per second), and the pressure difference that was monitored by the testing equipment, hydraulic conductivity, K, values were calculated for each sample using Darcy's Law:

$$Q = -K \times A \times (\mathrm{dh}/\mathrm{dl}),$$

where

K = hydraulic conductivity (in meters per second),
A = the area of the sample (in square meters),
dh = the difference in head across the sample (in meters), and
dl = the length of the sample (in meters).

These conductivity values were then converted to permeability (in square meters) using the following equation:

$$k = (K \times \mu)/(\rho \times g),$$

where

μ = viscosity (0.001 Pa·s),
ρ = density (1027 kg/m^3), and
g = the gravitational constant (9.81 m/s^2).

RESULTS

The measured samples from Site 1173 ranged in depth from 199.9 to 428.6 mbsf with lithologies consisting of silty claystone with moderate bioturbation (Moore, Taira, Klaus, et al., 2001). Samples from Site 1174 ranged in depth from 538.2 to 941.8 mbsf with lithologies consisting of silty and siliceous claystone.

Table T1 summarizes the permeability data for each sample, including the best estimate of permeability for each sample and the corresponding depths and initial porosities. Distribution of measured vertical permeabilities with depth are shown on Figures F4 and F5. Porosities were obtained from the shipboard data (Moore, Taira, Klaus, et al., 2001) and are not corrected for sediment rebound. We applied a variety of flow rates to each sample during the testing procedure to evaluate the repeatability of the measured permeabilities (Figs. F6, F7). The results from our testing indicate that the repeatability is good (Table T1).

Permeabilities were measured at varying effective stress values ranging from 0.24 to 0.62 MPa (Figs. F8, F9). In general, permeabilities decreased with increase in effective stress. Deeper samples showed less variation in permeability with increase in effective stress. Overall, the maximum change of permeability was less than an order of magnitude. Permeability values at the highest effective stress were used on Figures F4 and F5.

CONCLUSIONS

The highest permeability achieved for these samples was 6.45×10^{-17} m² for a sample with an initial porosity of 66% from the upper Shikoku Basin facies and the lowest permeability was 3.7×10^{-19} for a sample with an initial porosity of 35% from the lower Shikoku Basin facies.

ACKNOWLEDGMENTS

This research used samples and data provided by the Ocean Drilling Program (ODP). ODP is sponsored by the U.S. National Science Foundation (NSF) and participating countries under management of Joint Oceanographic Institutions (JOI), Inc. Funding for this research was provided by JOI/USSSP postcruise grant. We thank Brandon Dugan for helpful reviews of the manuscript and Kevin Hartl for his assistance in technical and laboratory procedures.

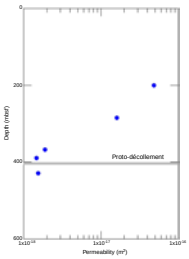

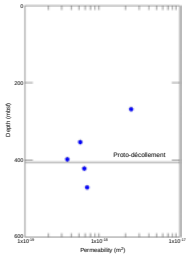

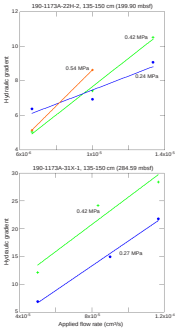

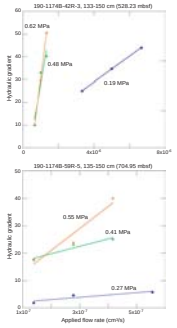

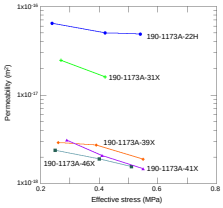

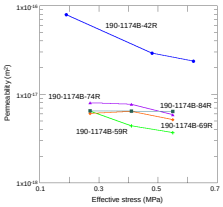

REFERENCES

ASTM, 1990. Standard test method for measurement of hydraulic conductivity of saturated porous materials using a flexible wall permeameter. Philadelphia (Am. Soc. Test. Mater.), D5084, 90:63–70.

Bolton, A., and Maltman, A., 1998. Fluid-flow pathways in actively deforming sediments: the role of pore fluid pressure and volume change. *Mar. Pet. Geol.,* 15:281–297.

Bolton, A., Maltman, A.J., and Fisher, Q., 2000. Anisotroptic permeability and bimodal pore-size distributions of fine-grained marine sediments. *Mar. Pet. Geol.,* 17:657–672.

Moore, G.F., Taira, A., Klaus, A., Becker, L., Boeckel, B., Cragg, A., Dean, A., Fergusson, C.L., Henry, P., Hirano, S., Hisamitsu, T., Hunze, S., Kastner, M., Maltman, A.J., Morgan, J.K., Murakami, Y., Saffer, D.M., Sánchez-Gómez, M., Screaton, E.J., Smith, D.C., Spivack, A.J., Steurer, J., Tobin, H.J., Ujiie, K., Underwood, M.B., and Wilson, M., 2001. New insights into deformation and fluid flow processes in the Nankai Trough accretionary prism: results of Ocean Drilling Program Leg 190. *Geochem. Geophys. Geosyst.,* 2:10.129/2001GC00166.

Moore, G.F., Taira, A., Klaus, A., et al., 2001. *Proc. ODP, Init. Repts.,* 190 [Online]. Available from World Wide Web: <http://www-odp.tamu.edu/publications/190_IR/190ir.htm>. [Cited 2003-03-12]

Figure F1. A location map of the Nankai Trough showing ODP Leg 190 (solid circles) and previous ODP and Deep Sea Drilling Project (DSDP) drill sites (solid squares). Contour interval = 100 m. (Moore, Taira, Klaus, et al., 2001).

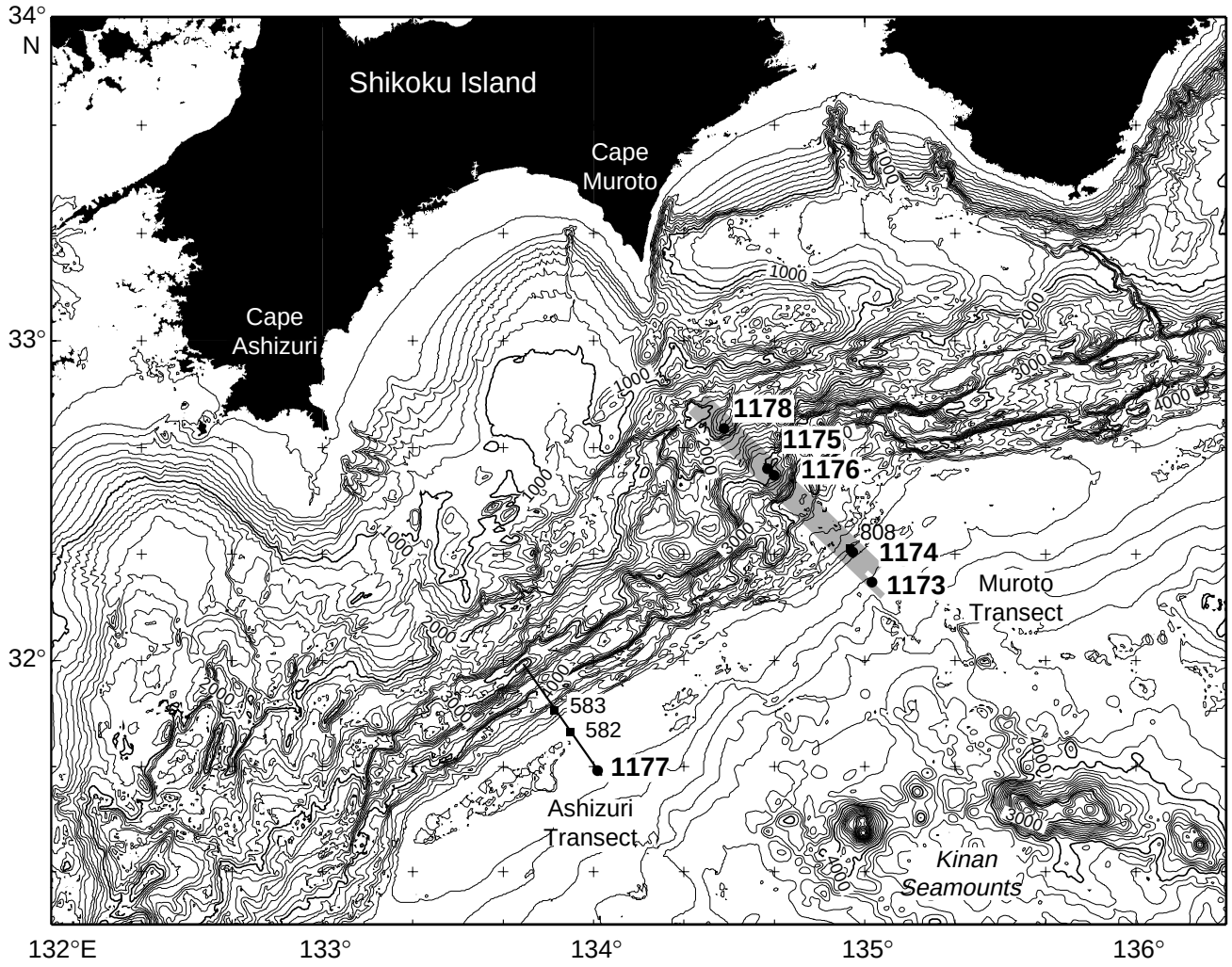

Figure F2. Laboratory setup for vertical permeability testing.

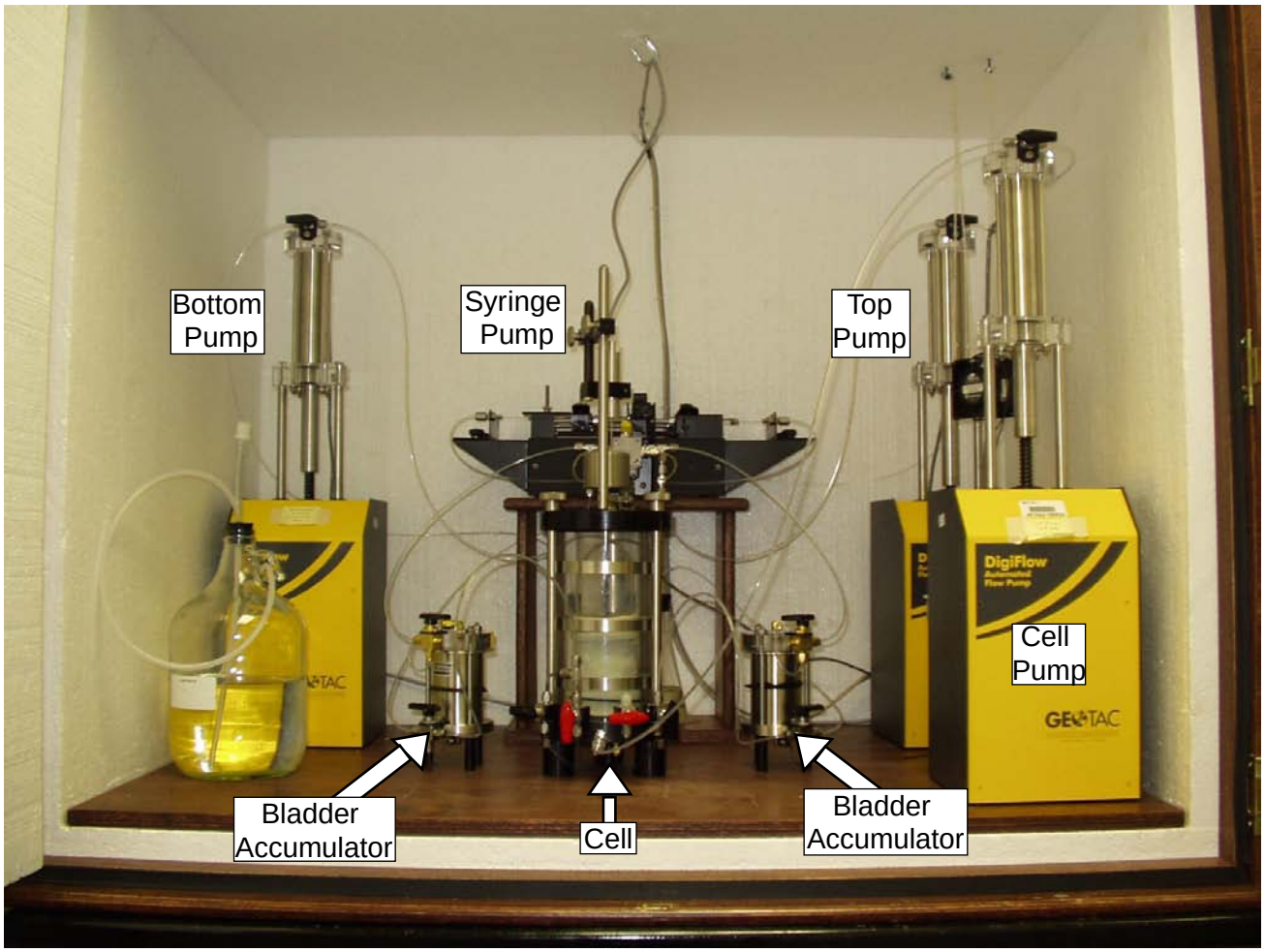

Figure F3. Constant-flow closed system used in permeability measurements. The permeameter cell is connected to the cell pump that infuses and withdraws water at a constant rate of flow across the sample. The absolute pressure transducers measure the pressure difference across the sample (head change) and the pressure difference between the cell fluid and the pore water fluid (effective stress).

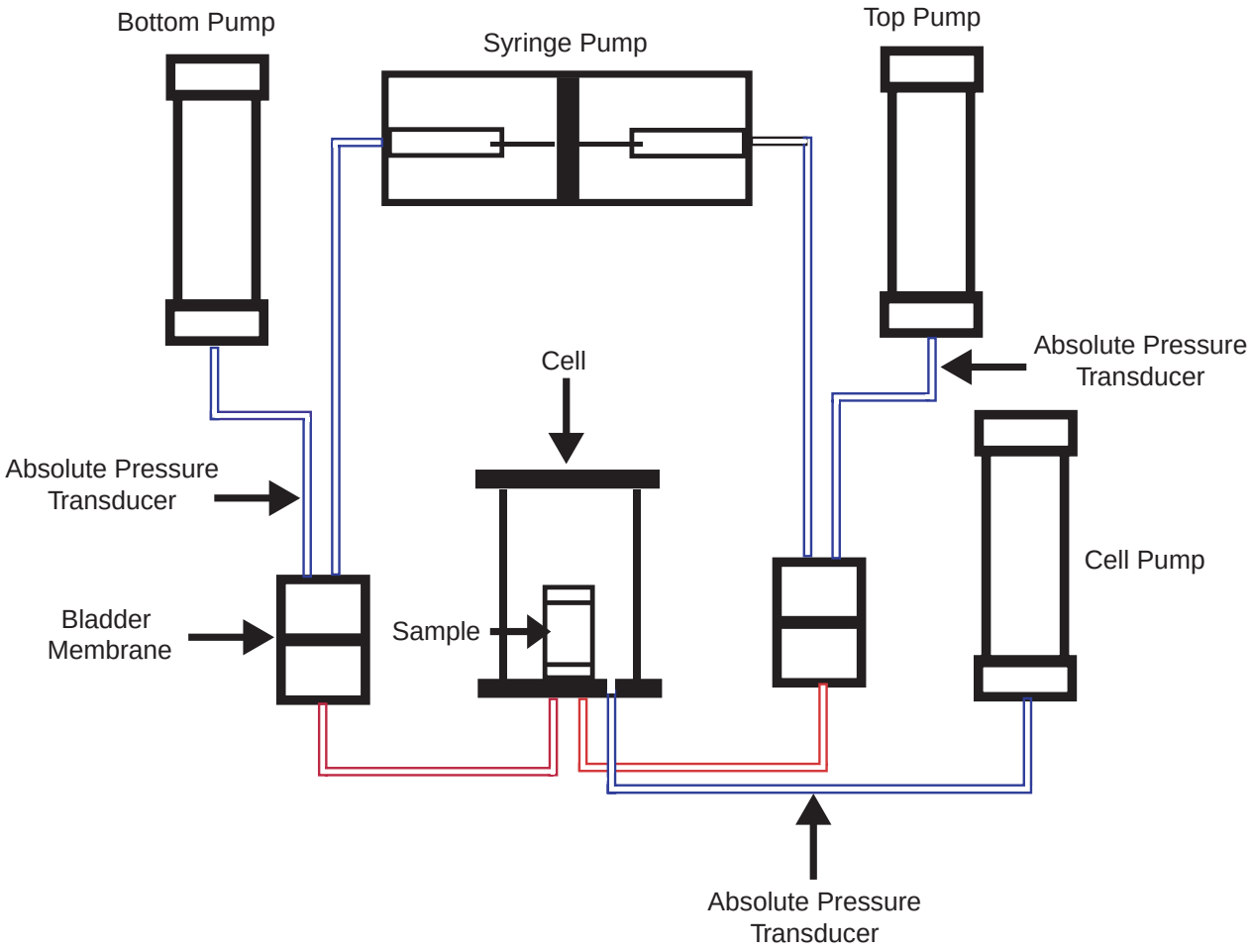

Figure F4. Distribution of measured vertical permeabilities with depth for samples collected from Leg 190, Site 1173. Permeability values at the highest effective stress are shown on the graph as they are considered closest to in situ vertical permeabilities.

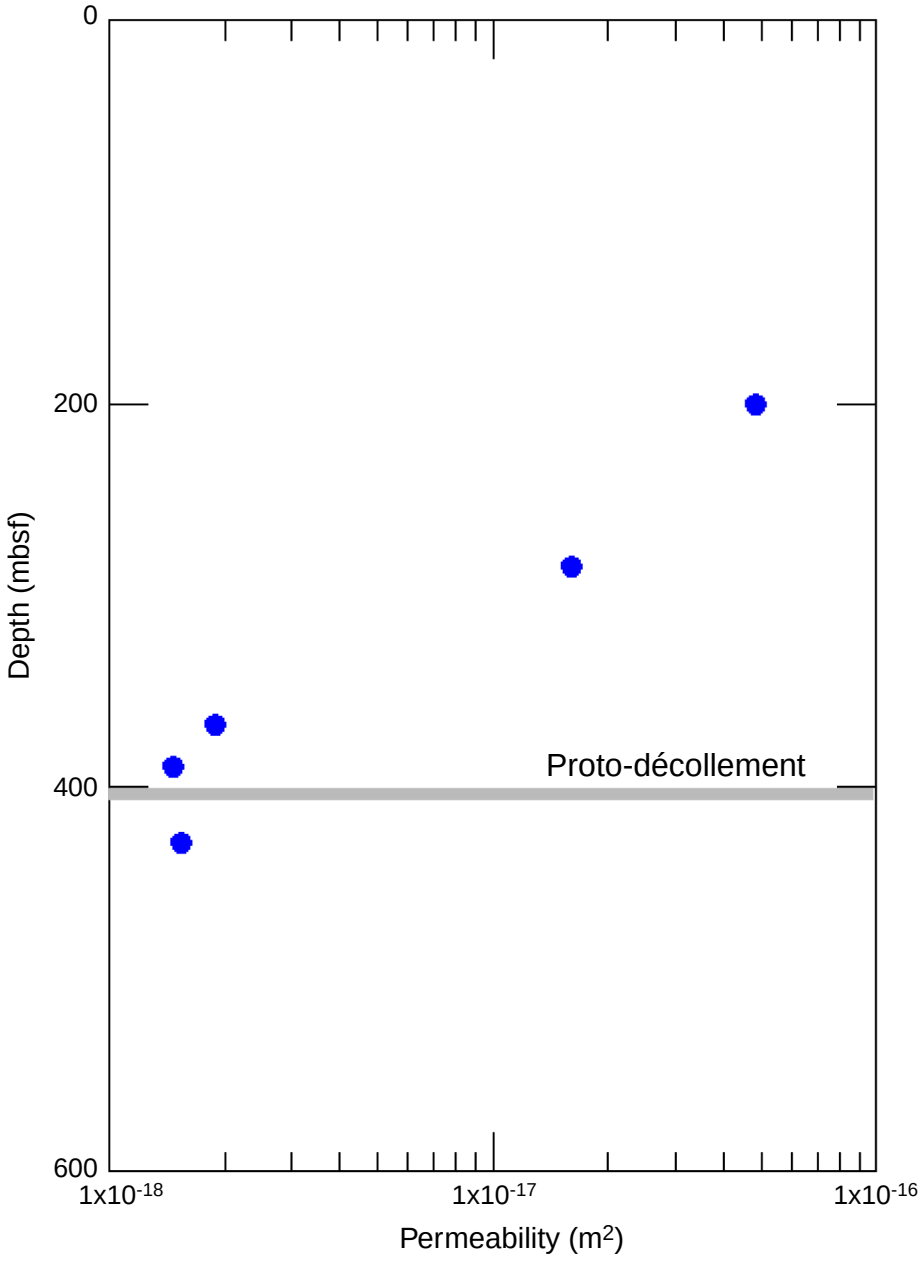

Figure F5. Distribution of measured vertical permeabilities with depth for samples collected from Leg 190, Site 1174. Permeability values at the highest effective stress are shown on the graph as they are considered closest to in situ vertical permeabilities.

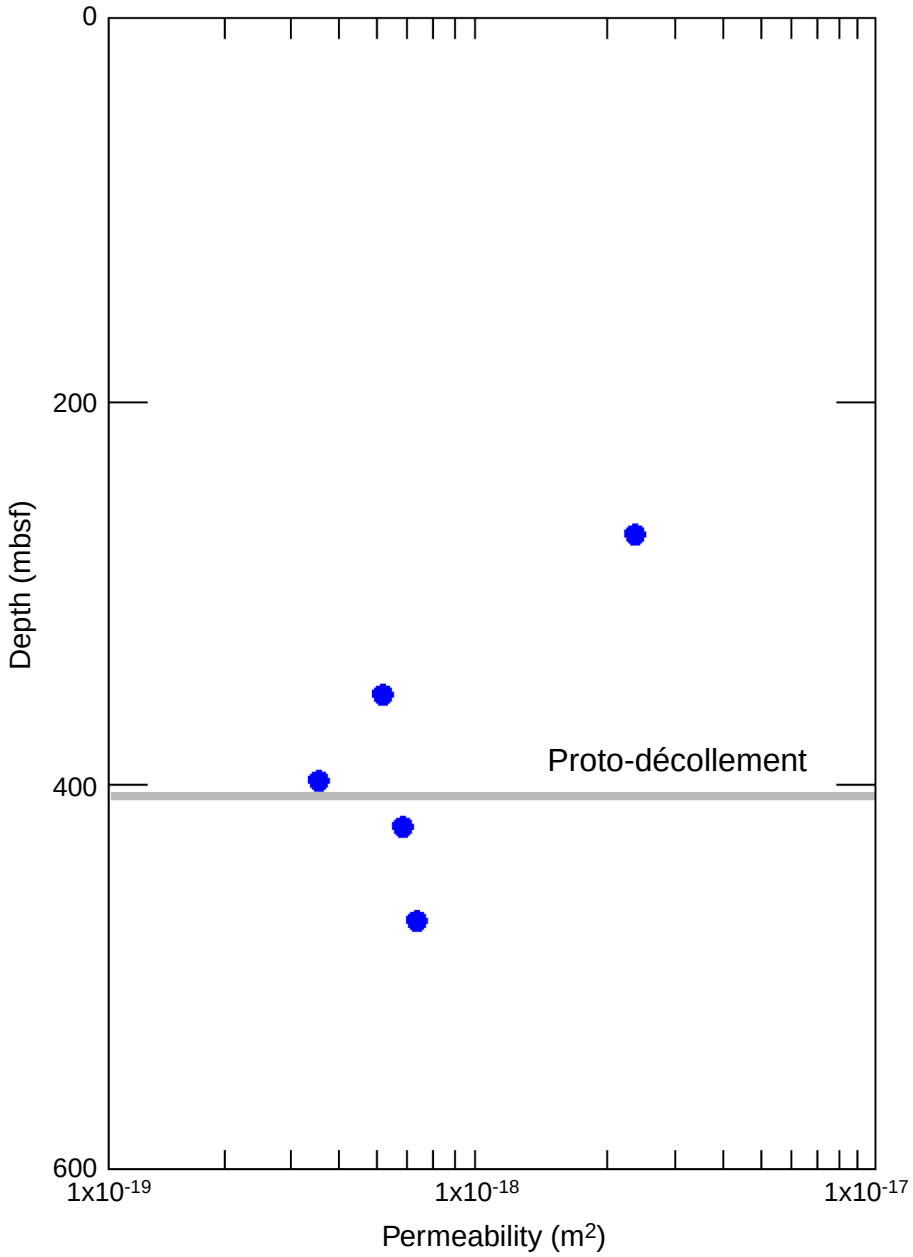

Figure F6. Hydraulic gradient as a function of applied flow rates for samples from Leg 190, Site 1173. Solid lines represent the linear trend line, and the solid patterns represent measured hydraulic gradients. (Continued on next two pages.)

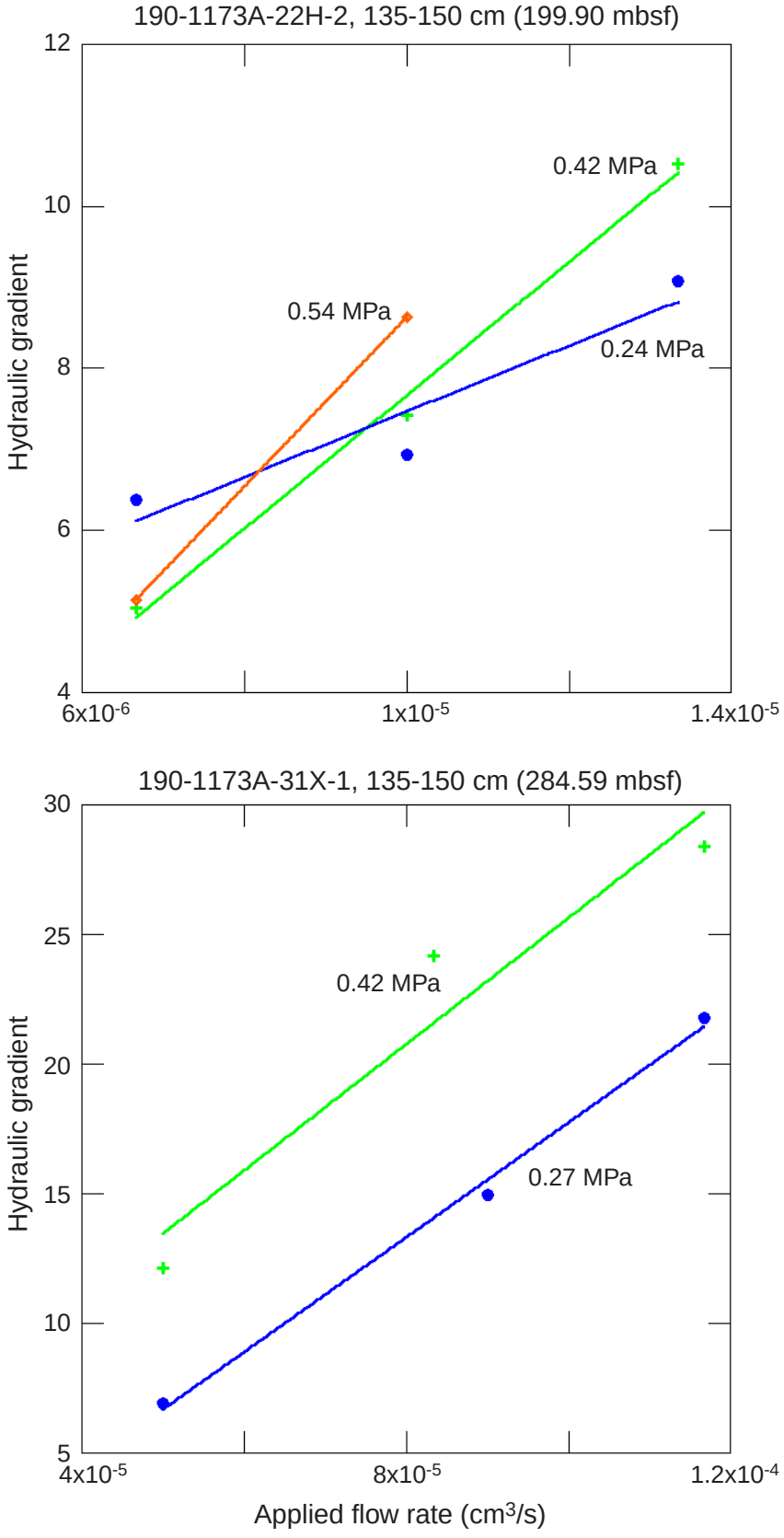

Figure F6 (continued).

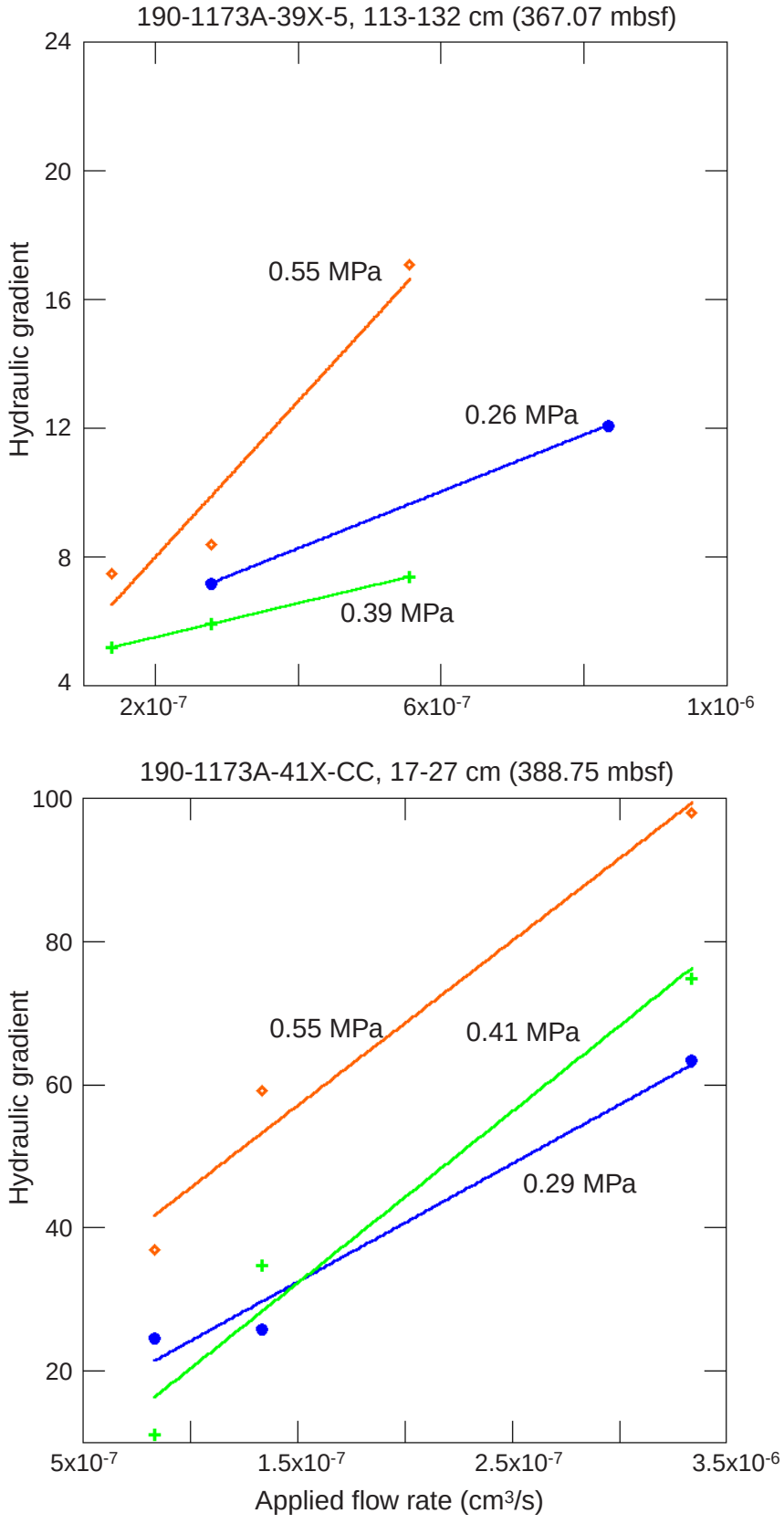

Figure F6 (continued).

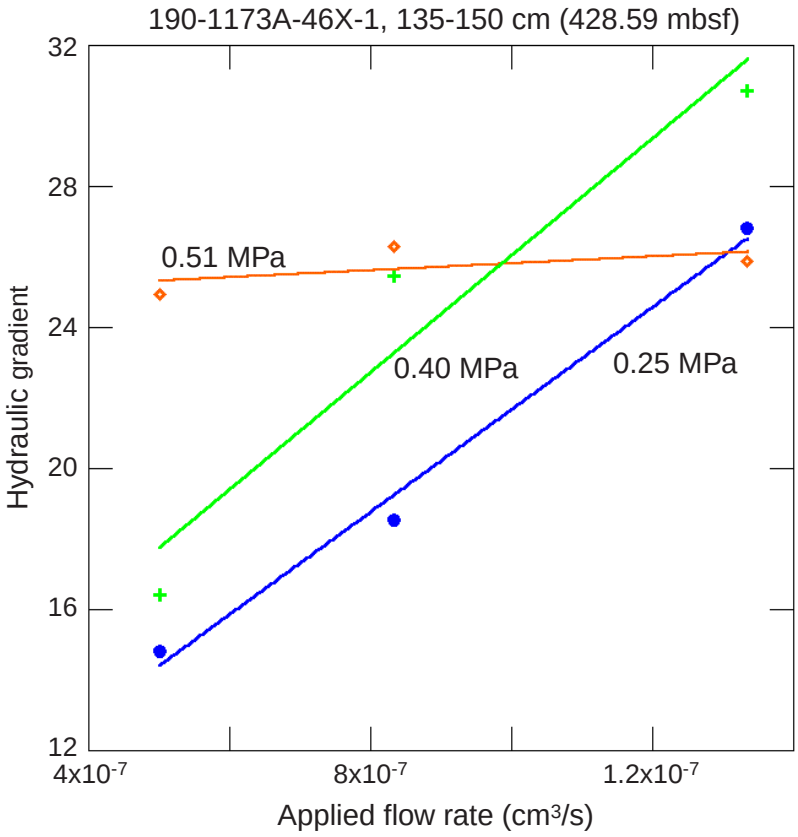

Figure F7. Hydraulic gradient as a function of applied flow rates for samples from Leg 190, Site 1174. Solid lines represent the linear trend line, and the solid patterns represent measured hydraulic gradients. (Continued on next two pages.)

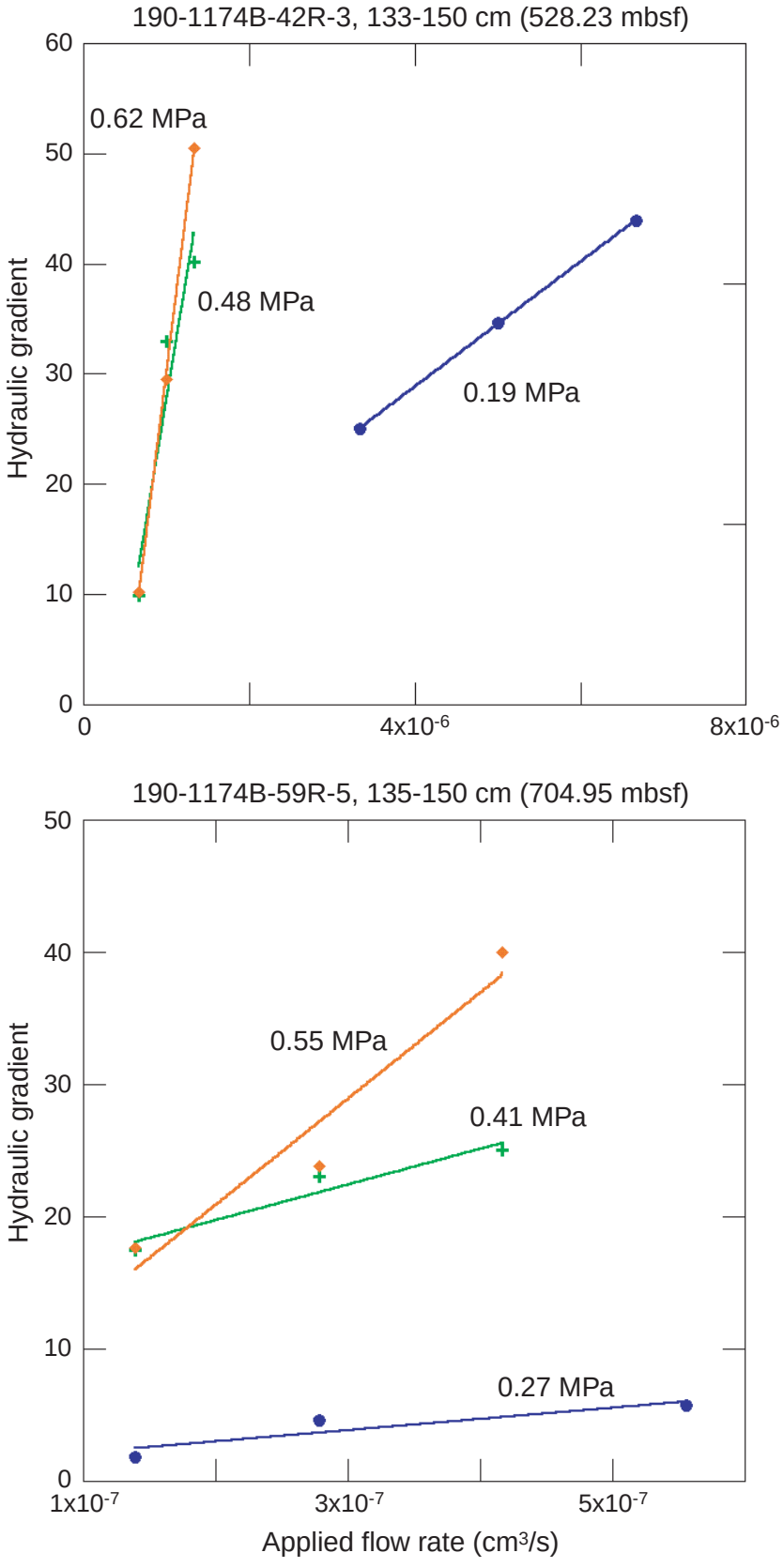

Figure F7 (continued).

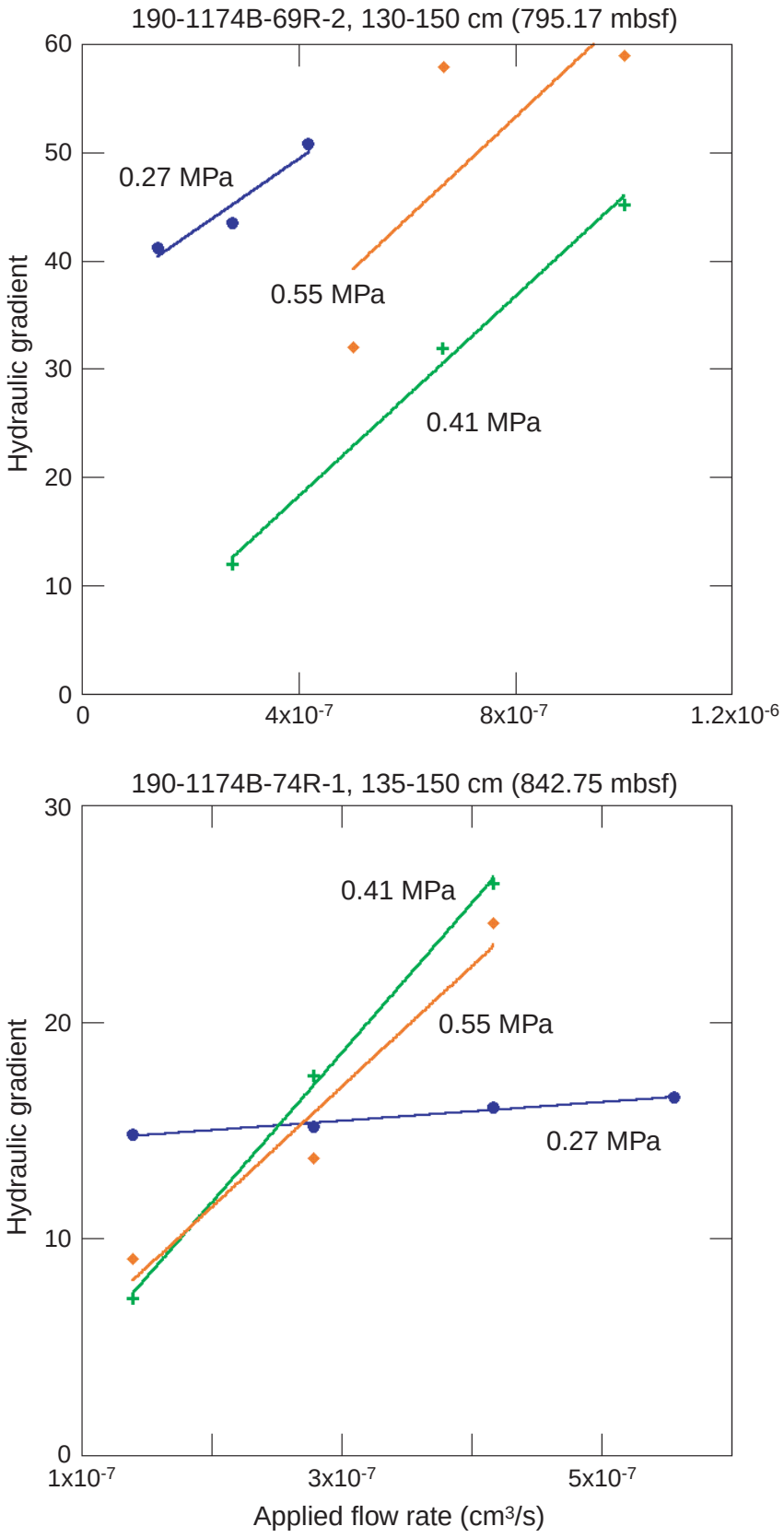

Figure F7 (continued).

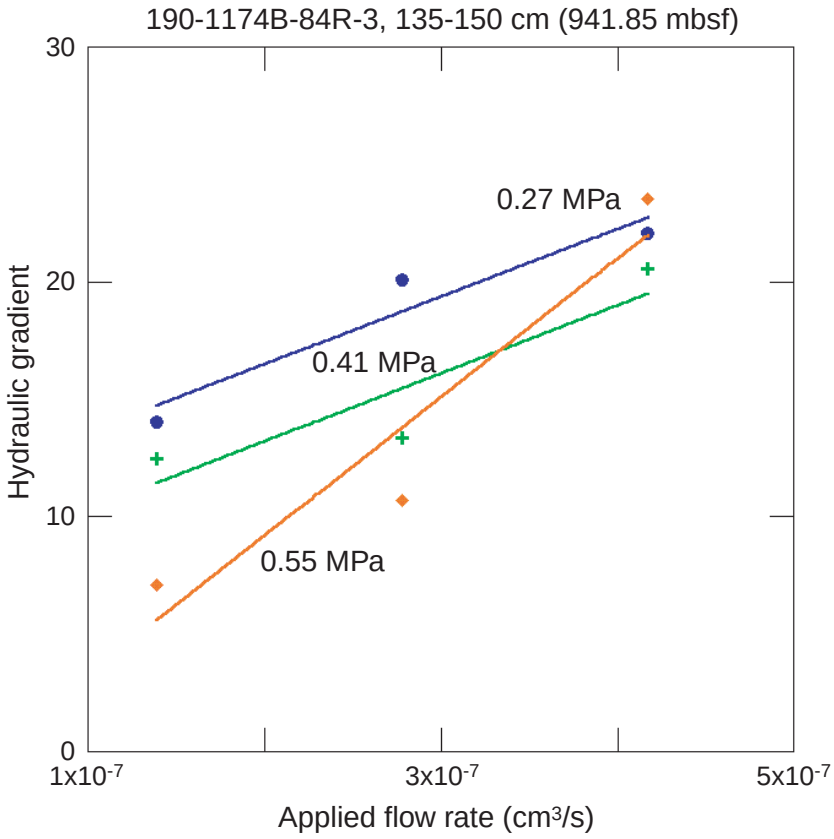

Figure F8. Permeability response to increasing effective stress for cores from Leg 190, Site 1173. Maximum effective stress used was 0.75 MPa.

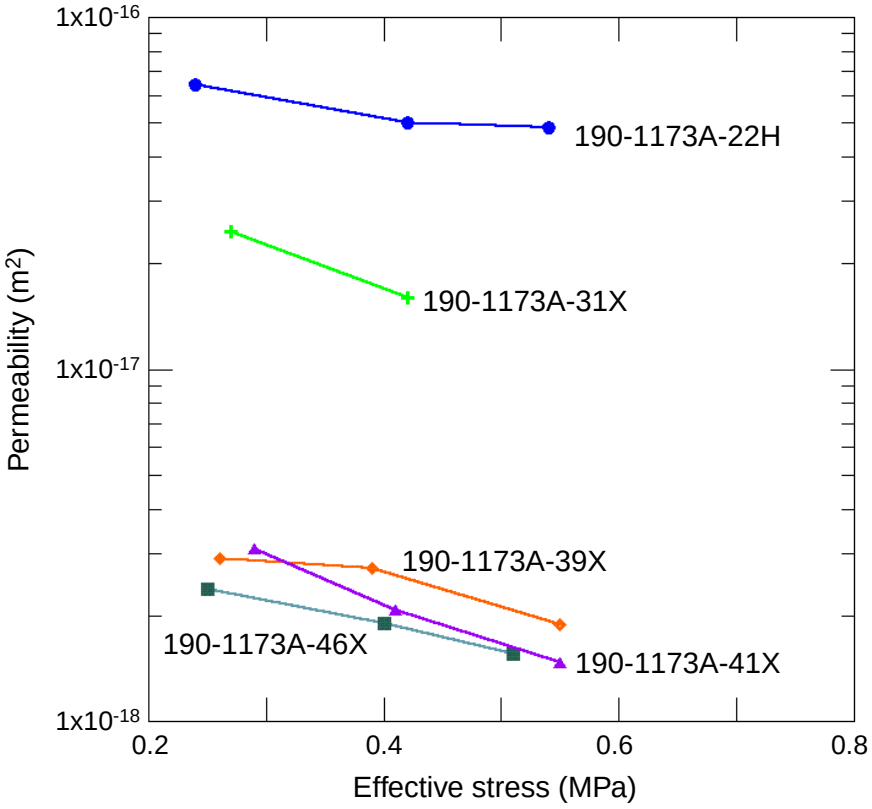

Figure F9. Permeability response to increasing effective stress for cores from Leg 190, Site 1174. Maximum effective stress used was 0.75 MPa.

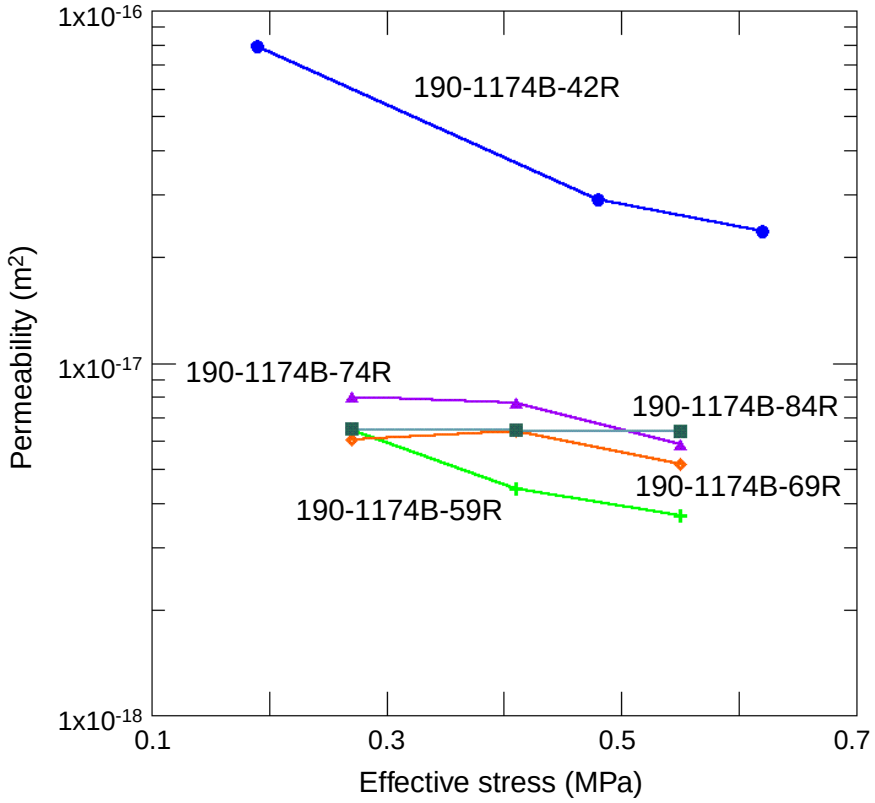

Table T1. Summary of permeability testing for samples from Leg 190, Sites 1173 and 1174. [N1] (See table notes. Continued on next page.)

Core, section, interval (cm)	Depth (mbsf)	Initial porosity (%)	Effective stress (σ_{eff}) (MPa)	Run	Flow rate (mL/s)	k (m^2)	K (cm/s)
190-1173A-							
22H-2, 135–150	199.9	65.5	0.24	1	6.66667×10^{-6}	6.90×10^{-17}	
				2	1.00000×10^{-5}	6.50×10^{-17}	
				3	1.33333×10^{-5}	5.90×10^{-17}	
					Average:	6.43×10^{-17}	7.66×10^{-8}
			0.42	1	6.66667×10^{-6}	4.70×10^{-17}	
				2	1.00000×10^{-5}	5.20×10^{-17}	
				3	1.33333×10^{-5}	5.20×10^{-17}	
					Average:	5.03×10^{-17}	3.78×10^{-8}
			0.54	1	6.66667×10^{-6}	5.00×10^{-17}	
				2	1.00000×10^{-5}	4.90×10^{-17}	
				3	1.33333×10^{-5}	4.70×10^{-17}	
					Average:	4.87×10^{-17}	2.97×10^{-9}
31X-1, 135–150	284.59	66.0	0.27	1	5.00000×10^{-5}	2.50×10^{-17}	
				2	8.33333×10^{-5}	2.40×10^{-17}	
				3	1.16667×10^{-4}	2.50×10^{-17}	
					Average:	4.87×10^{-17}	1.56×10^{-8}
			0.42	1	5.00000×10^{-5}	1.80×10^{-17}	
				2	8.33333×10^{-5}	1.60×10^{-17}	
				3	1.16667×10^{-4}	1.40×10^{-17}	
					Average:	1.60×10^{-17}	1.42×10^{-8}
39X-5, 113–132	367.07	49	0.26	1	5.55556×10^{-7}	4.24×10^{-18}	
				2	2.77778×10^{-7}	2.84×10^{-18}	
				3	8.33333×10^{-7}	2.28×10^{-18}	
				4	1.16667×10^{-6}	2.60×10^{-18}	
				5	1.66667×10^{-6}	2.60×10^{-18}	
					Average:	2.91×10^{-18}	4.02×10^{-9}
			0.39	1	1.38889×10^{-7}	1.64×10^{-18}	
				2	2.77778×10^{-7}	2.80×10^{-18}	
				3	5.55556×10^{-7}	2.02×10^{-18}	
				4	8.33333×10^{-7}	4.40×10^{-18}	
					Average:	2.72×10^{-18}	6.74×10^{-9}
			0.55	1	1.38889×10^{-7}	2.37×10^{-18}	
				2	2.77778×10^{-7}	2.00×10^{-18}	
				3	5.55556×10^{-7}	1.31×10^{-18}	
					Average:	1.89×10^{-18}	1.47×10^{-9}
41X-CC, 17–27	388.75	48.7	0.29	1	8.33333×10^{-7}	4.00×10^{-18}	
				2	1.33333×10^{-6}	2.80×10^{-18}	
				3	3.33333×10^{-6}	2.50×10^{-18}	
					Average:	3.10×10^{-18}	2.28×10^{-9}
			0.41	1	8.33333×10^{-7}	2.40×10^{-18}	
				2	1.33333×10^{-6}	1.80×10^{-18}	
				3	3.33333×10^{-6}	2.00×10^{-18}	
					Average:	2.07×10^{-18}	1.57×10^{-9}
			0.55	1	8.33333×10^{-7}	1.70×10^{-18}	
				2	1.33333×10^{-6}	1.50×10^{-18}	
				3	3.33333×10^{-6}	1.20×10^{-18}	
					Average:	1.47×10^{-18}	1.64×10^{-9}
46X-1, 135–150	428.59	48.5	0.25	1	5.00000×10^{-7}	2.50×10^{-18}	
				2	8.33333×10^{-7}	2.40×10^{-18}	
				3	1.33333×10^{-6}	2.20×10^{-18}	
					Average:	2.37×10^{-18}	2.48×10^{-9}
			0.40	1	5.00000×10^{-7}	2.00×10^{-18}	
				2	8.33333×10^{-7}	1.90×10^{-18}	
				3	1.33333×10^{-6}	1.80×10^{-18}	
					Average:	1.90×10^{-18}	2.17×10^{-9}
			0.51	1	5.00000×10^{-7}	1.60×10^{-18}	
				2	8.33333×10^{-7}	1.58×10^{-18}	
				3	1.33333×10^{-6}	1.48×10^{-18}	
					Average:	1.55×10^{-18}	3.65×10^{-8}

Table T1 (continued).

Core, section, interval (cm)	Depth (mbsf)	Initial porosity (%)	Effective stress (σ_{eff}) (MPa)	Run	Flow rate (mL/s)	k (m^2)	K (cm/s)
190-1174B-							
42R-3, 133–150	538.23	37.9	0.19	1	3.33333×10^{-6}	7.71×10^{-18}	
				2	5.00000×10^{-6}	8.17×10^{-18}	
				3	6.66667×10^{-6}	7.99×10^{-18}	
					Average:	7.95×10^{-18}	8.35×10^{-9}
			0.48	1	6.66667×10^{-7}	4.65×10^{-18}	
				2	1.00000×10^{-6}	1.90×10^{-18}	
				3	1.33333×10^{-6}	2.17×10^{-18}	
					Average:	2.91×10^{-18}	1.04×10^{-9}
			0.62	1	6.66667×10^{-7}	3.18×10^{-18}	
				2	1.00000×10^{-6}	2.20×10^{-18}	
				3	1.33333×10^{-6}	1.70×10^{-18}	
					Average:	2.36×10^{-18}	7.89×10^{-10}
59R-5, 135–150	704.95	34.9	0.27	1	1.38889×10^{-7}	3.92×10^{-19}	
				2	2.77778×10^{-7}	7.09×10^{-19}	
				3	5.55556×10^{-7}	8.44×10^{-19}	
					Average:	6.48×10^{-19}	4.68×10^{-9}
			0.41	1	1.38889×10^{-7}	2.58×10^{-19}	
				2	2.77778×10^{-7}	3.95×10^{-19}	
				3	4.16666×10^{-7}	6.70×10^{-19}	
					Average:	4.41×10^{-19}	1.47×10^{-9}
			0.55	1	1.38889×10^{-7}	2.22×10^{-19}	
				2	2.77778×10^{-7}	4.70×10^{-19}	
				3	4.16666×10^{-7}	4.11×10^{-19}	
					Average:	3.68×10^{-19}	4.94×10^{-10}
69R-2, 130–150	795.17	32.6	0.27	1	2.77778×10^{-7}	6.78×10^{-19}	
				2	4.16667×10^{-7}	6.30×10^{-19}	
				3	5.55556×10^{-7}	5.07×10^{-19}	
					Average:	6.05×10^{-19}	1.03×10^{-9}
			0.41	1	2.77778×10^{-7}	7.01×10^{-19}	
				2	6.66667×10^{-7}	6.10×10^{-19}	
				3	1.00000×10^{-6}	6.13×10^{-19}	
					Average:	6.41×10^{-19}	7.73×10^{-10}
			0.55	1	5.00000×10^{-7}	5.11×10^{-19}	
				2	6.66667×10^{-7}	4.61×10^{-19}	
				3	1.00000×10^{-6}	5.80×10^{-19}	
					Average:	5.17×10^{-19}	7.63×10^{-10}
74R-1, 1 35–150	842.75	34.1	0.27	1	1.38889×10^{-7}	3.82×10^{-19}	
				2	2.77778×10^{-7}	6.98×10^{-19}	
				3	5.55556×10^{-7}	1.32×10^{-18}	
					Average:	8.00×10^{-19}	8.28×10^{-10}
			0.41	1	1.38889×10^{-7}	1.14×10^{-18}	
				2	2.77778×10^{-7}	6.04×10^{-19}	
				3	4.16667×10^{-7}	5.67×10^{-19}	
					Average:	7.70×10^{-19}	5.19×10^{-10}
			0.55	1	1.38889×10^{-7}	6.67×10^{-19}	
				2	2.77778×10^{-7}	5.52×10^{-19}	
				3	4.16666×10^{-7}	5.45×10^{-19}	
					Average:	5.88×10^{-19}	6.45×10^{-10}
84R-3, 135–150	941.85	35.7	0.27	1	1.38889×10^{-7}	6.64×10^{-19}	
				2	2.77778×10^{-7}	6.17×10^{-19}	
				3	4.16666×10^{-7}	6.76×10^{-19}	
					Average:	6.52×10^{-19}	1.26×10^{-9}
			0.41	1	1.38889×10^{-7}	7.30×10^{-19}	
				2	2.77778×10^{-7}	5.67×10^{-19}	
				3	4.16666×10^{-7}	6.41×10^{-19}	
					Average:	6.46×10^{-19}	1.25×10^{-9}
			0.55	1	1.38889×10^{-7}	6.14×10^{-19}	
				2	2.77778×10^{-7}	6.80×10^{-19}	
				3	4.16666×10^{-7}	6.27×10^{-19}	
					Average:	6.40×10^{-19}	6.15×10^{-10}

Notes: k = permeability, K = hydraulic conductivity. K is calculated from the slope of hydraulic gradient vs. flow rate plots.

CHAPTER NOTE*

N1. 27 October 2004—After this chapter was published, several errors were found in Table **T1.** The unit for hydraulic conductivity (*K*) was changed, and the values in the *K* column also changed. The table note was missing in the World Wide Web PDF version when the chapter was first published; the table note has now been restored along with an additional note from the author.

*Dates reflect file corrections or revisions.